Understanding and Fine Tuning the Propensity of ATP-Driven Liquid-Liquid Phase Separation with Oligolysine

Qiang Zhu, Yongxian Wu, and Ray Luo*

Department of Molecular Biology and Biochemistry, Chemical and Biomolecular Engineering, Materials Science and Engineering, and Biomedical Engineering, University of California, Irvine, Irvine, California 92697, United States

E-mail: rluo@uci.edu

Contents

S1 Summary of charge parameters for oligolysine

Table S1: Summary of the charge parameters for oligolysine studied in this work.

Description	bead type	charge (e)
SC1 (sidechain)	C3	0
SC2 (sidechain)	Qd	1
BB (backbone)	P5	0
BB (backbone N-ter)	Qd	1
BB (backbone C-ter)	Qa	-1

S2 System Summary

Table S2: Summary of the composition of systems studied in this work together with their simulation time

No.	Name	# Oligolysine	# ATP	Ionic Conc. (M)	Time (μs)	# Parallel
1	K_4	20	0	0.15/0.50/0.75/1.00	8	3
2	K_8	20	0	0.15/0.50/0.75/1.00	8	3
3	K_{16}	20	0	0.15/0.50/0.75/1.00	8	3
4	K_{24}	20	0	0.15/0.50/0.75/1.00	8	3
5	K_{32}	20	0	0.15/0.50/0.75	8	1
6	K_{40}	20	0	0.15/0.50/0.75	8	3
7	K_4	100	0	0.15/0.50/0.75/1.00	8	1
8	K_8	100	0	0.15/0.50/0.75/1.00	8	1
9	K_{16}	100	0	0.15/0.50/0.75/1.00	8	1
10	K_{24}	100	0	0.15/0.50/0.75/1.00	8	1
11	K_{32}	100	0	0.15/0.50/0.75	8	1
12	K_{40}	100	0	0.15/0.50/0.75	8	1
13	K_4/ATP	20	20	0.15/0.50/0.75/1.00	8	3
14	K_8/ATP	20	20	0.15/0.50/0.75/1.00	8	3
15	K_{16}/ATP	20	20	0.15/0.50/0.75/1.00	8	3
16	K_{24}/ATP	20	20	0.15/0.50/0.75/1.00	8	3
17	K_{32}/ATP	20	20	0.15/0.50/0.75	8	1
18	K_{40}/ATP	20	20	0.15/0.50/0.75	8	3
19	K_4	100	100	0.15/0.50/0.75/1.00	8	1
20	K_8	100	100	0.15/0.50/0.75/1.00	8	1
21	K_{16}	100	100	0.15/0.50/0.75/1.00	8	1
22	K_{24}	100	100	0.15/0.50/0.75/1.00	8	1
23	K_{32}	100	100	0.15/0.50/0.75	8	1
24	K_{40}	100	100	0.15/0.50/0.75	8	1
25	K_4 [a]	20	0	0.15	8	1
26	K_8 [a]	20	0	0.15	8	1
27	K_{16} [a]	20	0	0.15	8	1
28	K_{24} [a]	20	0	0.15	8	1
29	K_{40} [a]	20	0	0.15	8	1
30	K_4/ATP [a]	20	20	0.15	8	1
31	K_8/ATP [a]	20	20	0.15	8	1
32	K_{16}/ATP [a]	20	20	0.15	8	1
33	K_{24}/ATP [a]	20	20	0.15	8	1
34	K_{32}/ATP [a]	20	20	0.15	8	1
35	K_{40}/ATP [a]	20	20	0.15	8	1
36	K_4/ATP	200	20	0.15	8	1
37	K_4/ATP	1000	100	0.15	8	1
38	K_{40}/ATP [b]	20	20	0.15	8	1
39	K_{40}/ATP [b]	100	100	0.15	8	1

[a] where oligolysine is treated as neutral while main-chain beads at N and C terminal are assigned positive and negative charges.

[b] The vibrational degree of freedom was restricted by forming a cyclic peptide, leaving all other parameters intact with linear one.

S3 Radius of gyration

Table S3: Radius of gyration (r^2_{gyr}) taking different ionic concentrations and addition of ATP into considerations. The standard deviations are shown in parentheses.

K_n	ionic conc. (M)	pressure (bar)	r^2_{gyr} (Å^2)	
			w	w/o
K_4	0.15	1.0	5.34 (0.31)	5.34 (0.32)
K_4	0.50	1.0	5.30 (0.31)	5.34 (0.32)
K_4	0.75	1.0	5.31 (0.31)	5.34 (0.32)
K_4	1.00	1.0	5.33 (0.31)	5.34 (0.32)
K_8	0.15	1.0	7.10 (0.50)	7.12 (0.54)
K_8	0.50	1.0	7.11 (0.48)	7.12 (0.54)
K_8	0.75	1.0	7.13 (0.49)	7.10 (0.54)
K_8	1.00	1.0	7.14 (0.49)	7.09 (0.54)
K_{16}	0.15	1.0	10.00 (1.04)	10.52 (1.02)
K_{16}	0.50	1.0	9.97 (1.01)	10.46 (1.04)
K_{16}	0.75	1.0	9.98 (1.02)	10.40 (1.04)
K_{16}	1.00	1.0	9.96 (1.06)	10.30 (1.06)
K_{24}	0.15	1.0	12.76 (1.71)	13.77 (1.44)
K_{24}	0.50	1.0	12.57 (1.72)	13.70 (1.44)
K_{24}	0.75	1.0	12.51 (1.72)	13.61 (1.44)
K_{24}	1.00	1.0	12.35 (1.71)	13.48 (1.44)
K_{40}	0.15	1.0	17.78 (2.84)	19.34 (2.42)
K_{40}	0.50	1.0	17.60 (2.99)	19.25 (2.40)
K_{40}	0.75	1.0	17.77 (2.77)	19.03 (2.39)

S4 Dihedral formed between two adjacent residues

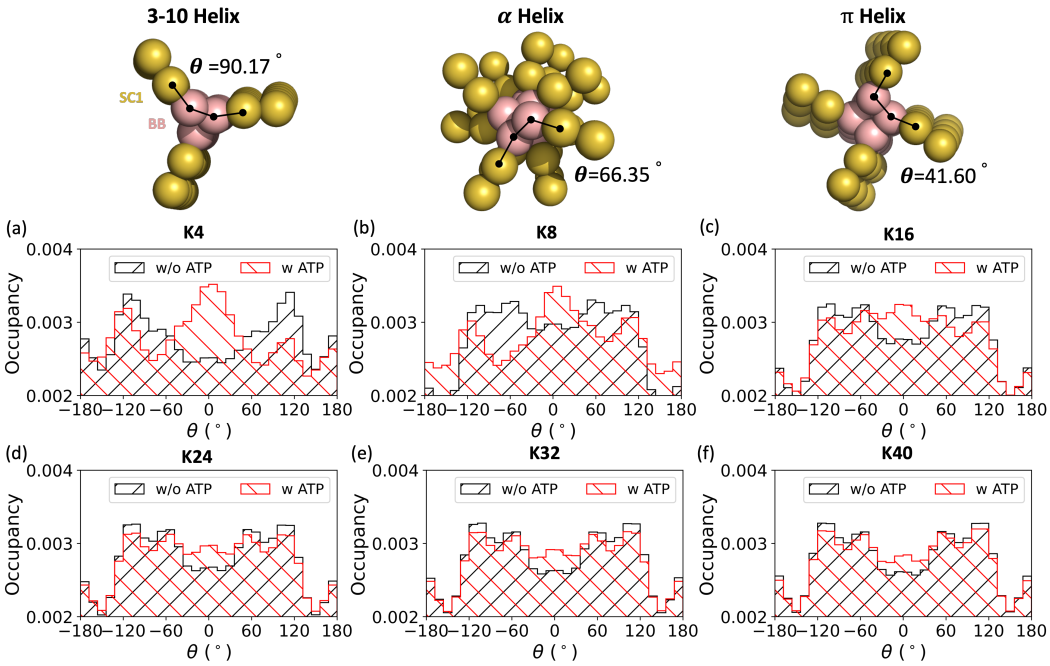

Figure S1: Distribution of dihedrals formed between two adjacent lysine residues of different oligolysine lengths with and without ATPs. (a)-(f) correspond to oligolysine of length 4, 8, 16, 24, 32, and 40, respectively. Top shown are three representative structures of 3-10 Helix, α-Helix, and π-Helix generated by Avogadro[1] and then mapped into coarse-grained ones using the MARITINI model (version 2.2).[2] Together shown are their corresponding dihedrals formed between two adjacent residues.

S5 Radial Distribution Function

S5.1 Effects of ionic concentrations in the presence of ATPs

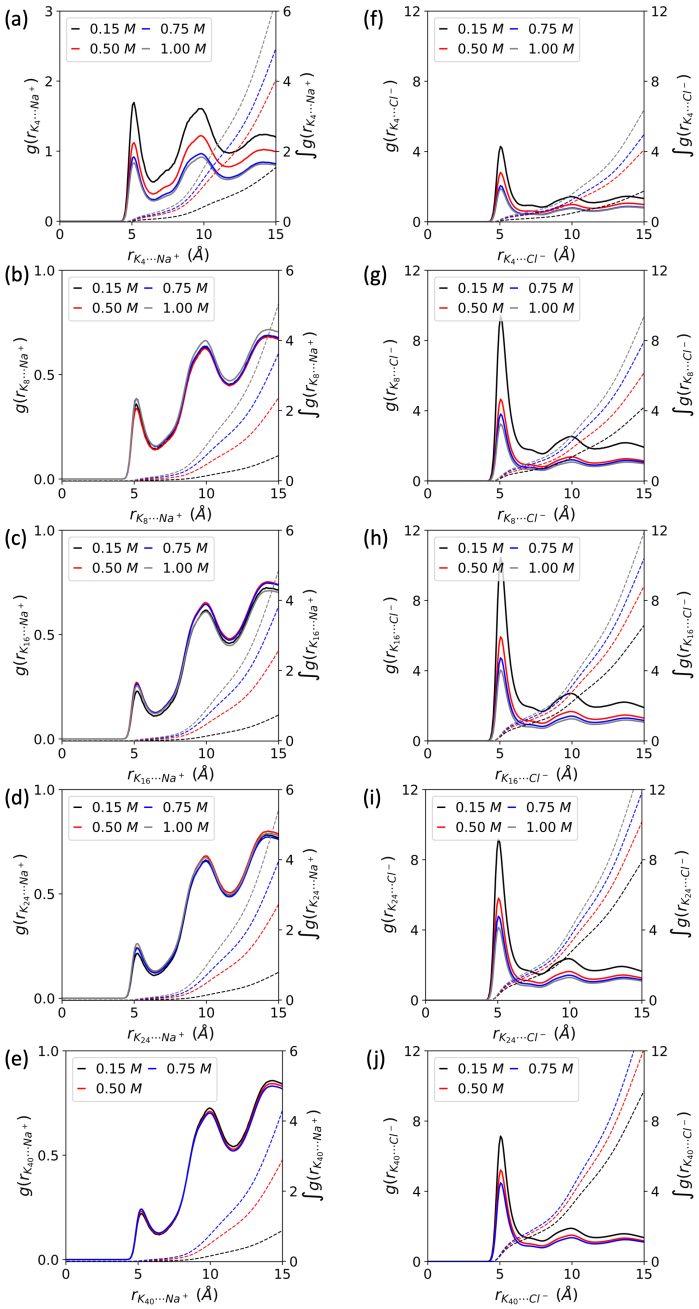

Figure S2: Effects of ionic concentration on the radial distribution function between (a-e) Na^+ and (f-j) Cl^- and oligolysine of different length oligolysine in the case where ATP was added. Together shown are their corresponding integrations in dashed lines.

S5.2 Effects of ionic concentrations in the absence of ATPs

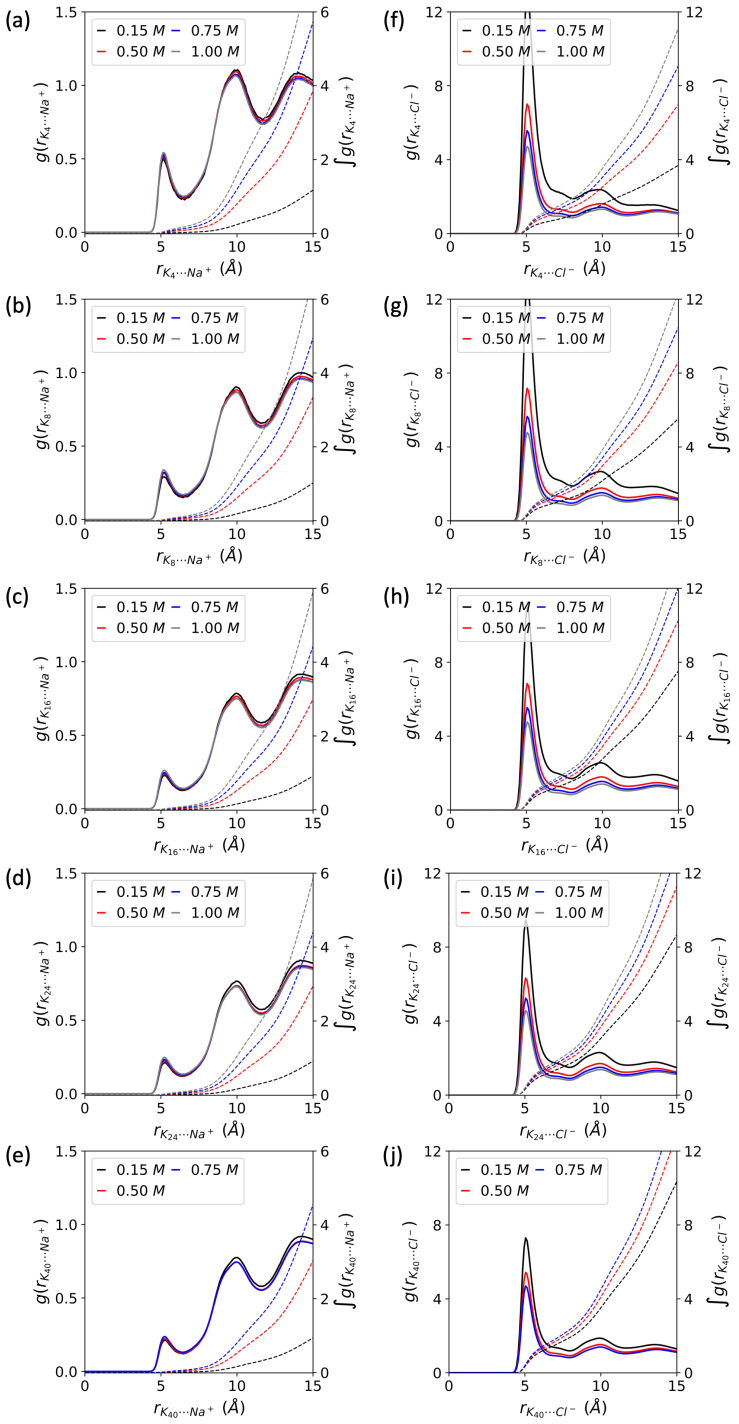

Figure S3: Effects of ionic concentration on the radial distribution function between (a-e) Na^+ and (f-j) Cl^- and oligolysine of different length oligolysine in the absence of ATP. Together shown are their corresponding integrations in dashed lines.

S5.3 Effects of ATP exerted on RDF between oligolysine and ions

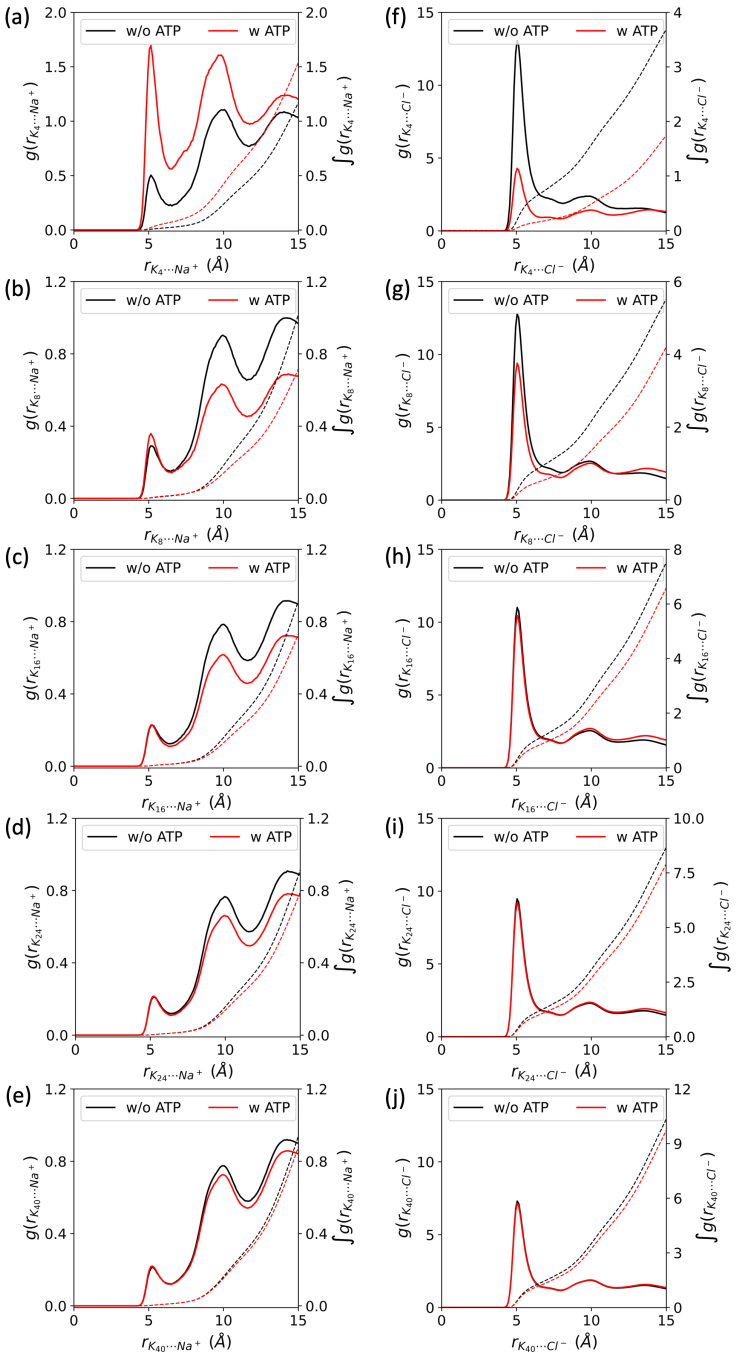

Figure S4: Radial distribution function between (a-d) Na^+ and (e-h) Cl^- and oligolysine of different length oligolysine with (red line) or without (black line) the addition of ATP at the ionic concentration of 0.15 M. Together shown are their corresponding integrations in dashed lines.

S6 Determination of the threshold distance

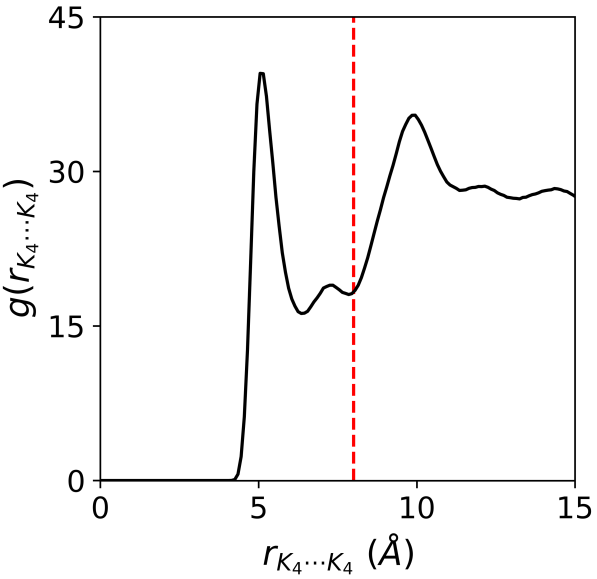

Figure S5: The radial distribution function between any two paired oligolysines of length 4 (K_4). Red dashed line represents criterion of 8 angstrom that we employed in this work.

The threshold distance for categorizing each oligolysine as being in the same cluster is derived from the radial distribution function between any two paired oligolysines. (Figure S5) The radial distribution shown here is averaged over any two paired oligolysines that are treated as intact one. Here, we just show the results for oligolysine of length 4. The first peak denotes an interaction could be detected between paired oligolysine. Consequently, a somewhat larger distance (end of second peak valley, red dashed line shown in Figure S5) is chosen for judging whether any two oligolysines could aggregate.

S7 Diffusion Coefficient

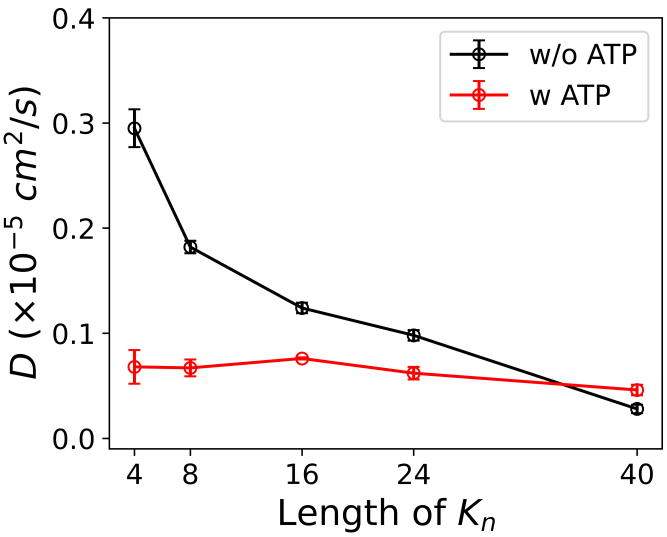

Figure S6: Diffusion coefficient (D) as a function of length of oligolysine with (w, red line) and without (w/o, black line) the existence of ATP.

S8 Solvent Accessible Surface Area

The solvent accessible surface area was estimated with the help of VMD,[3] where the solvent probe radii is set to be 1.4 Å.

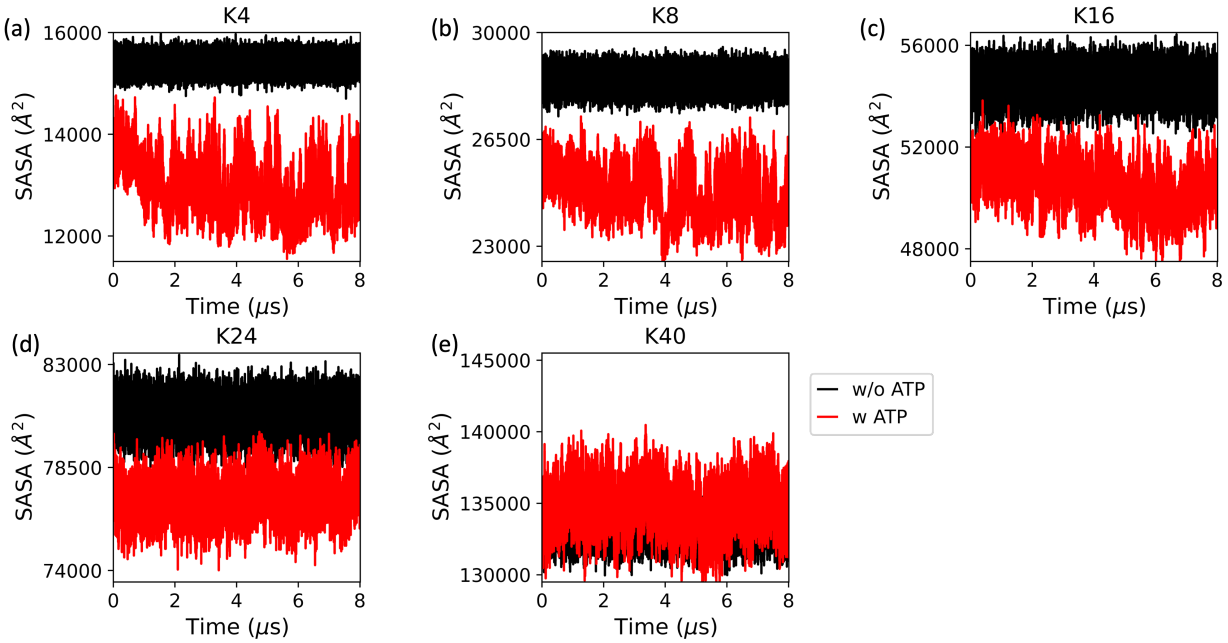

Figure S7: Evolution of Solvent accessible surface area (SASA) of oligolysine as a function of time with or without ATP: (a) K_4; (b) K_8; (c) K_{16}; (d) K_{24}; (e) K_{40}

S9 Energy decomposition

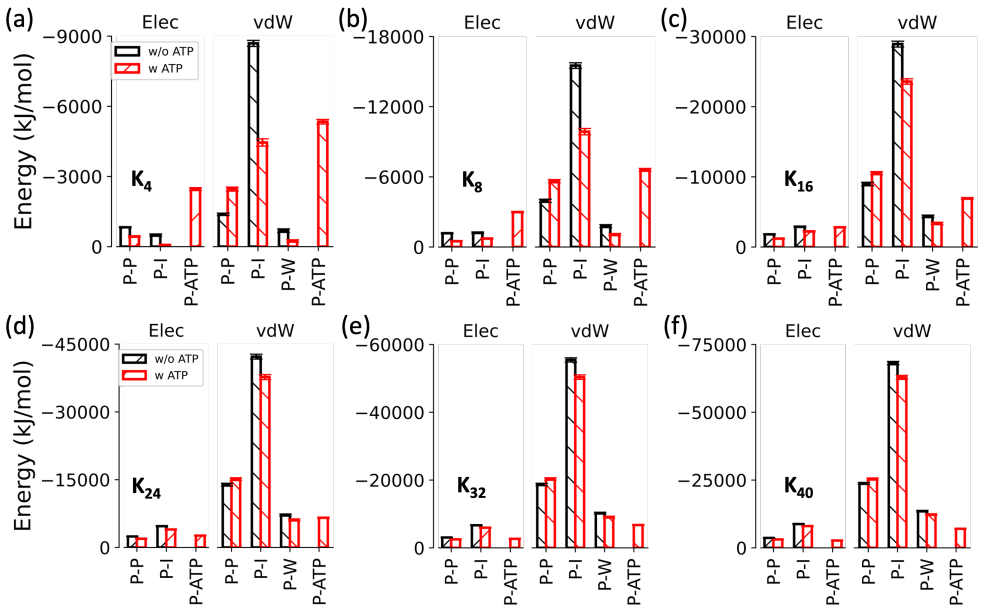

Figure S8: The interaction energies for Coulomb (elec) and LJ (vdW) term formed between protein-protein (P-P), protein-ions (P-I), protein-water (P-W), and protein-ATP (P-ATP) of different oligolysine lengths with and without addition of ATPs.

S10 Investigation of the preference for high flexibility

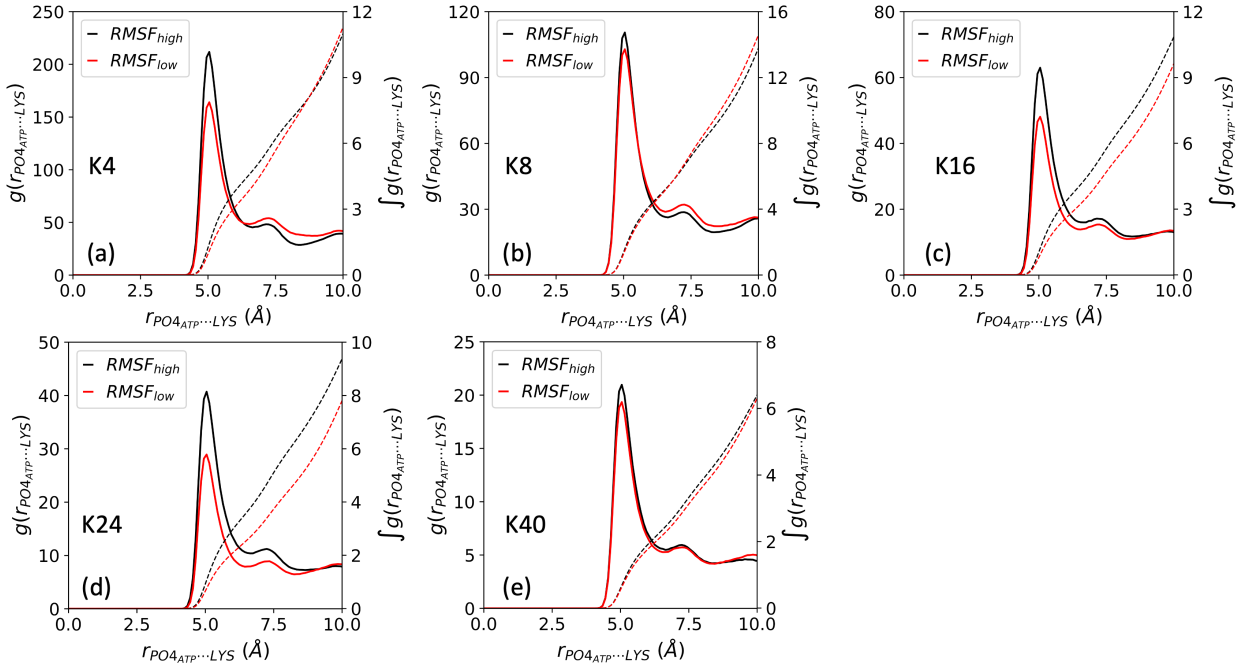

Figure S9: The radial distribution function between the phosphate group of ATP ($PO4_{ATP}$) and oligolysine (LYS) of high and low fluctuating region. (a) - (e) represent oligolysine of length 4, 8, 16, 24, and 40, respectively. Integration over the distribution is presented in dashed line. For oligolysine of length 4 (K_4), first and last LYS are picked as high fluctuating region, second and third are selected as low fluctuating region. For K_8, resid # 1, 4, 5, 8 are for high fluctuating region and 2, 3, 6, 7 for low fluctuating region; For K_{16}, resid # 1, 2, 8, 9, 15, 16 are for high fluctuating region and 3, 4, 5, 12, 13, 14 for low fluctuating region; For K_{24}, resid # 1, 2, 3, 11, 12, 22, 23, 24 are for high fluctuating region and 4, 5, 6, 7, 17, 18, 19, 20 for low fluctuating region; For K_{40}, resid # 1, 2, 3, 4, 19, 20, 37, 38, 39, 40 are for high fluctuating region and 8, 9, 10, 11, 12, 30, 31, 32, 33, 34 for low fluctuating region.

S11 Effects of ATPs and ionic concentrations on the propensity of LLPS derived from large-size systems

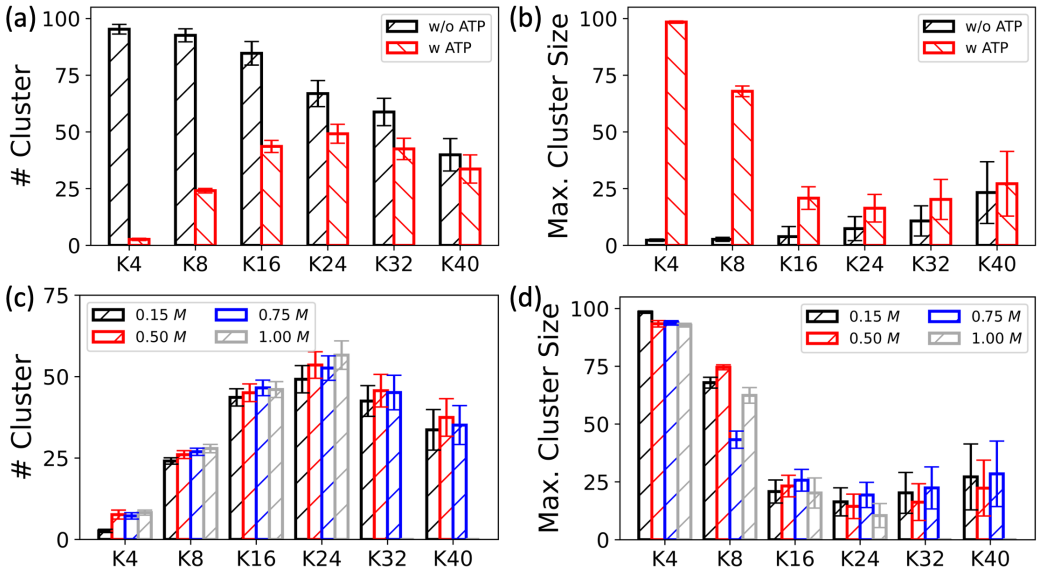

Figure S10: Effects of ATPs and ionic concentrations on the propensity to form LLPS in systems containing 100 oligolysines and ATPs. The effect of ATP exerts on (a) the number of clusters and (b) the maximum cluster size over systems of different oligolysine lengths (K_n), with the ionic concentration maintained at 0.15 M; The impact of different ionic concentrations caused on (c) the number of clusters and (d) the maximum cluster size in systems of oligolysines paired with ATPs.

S12 Final snapshots extracted from large-size systems

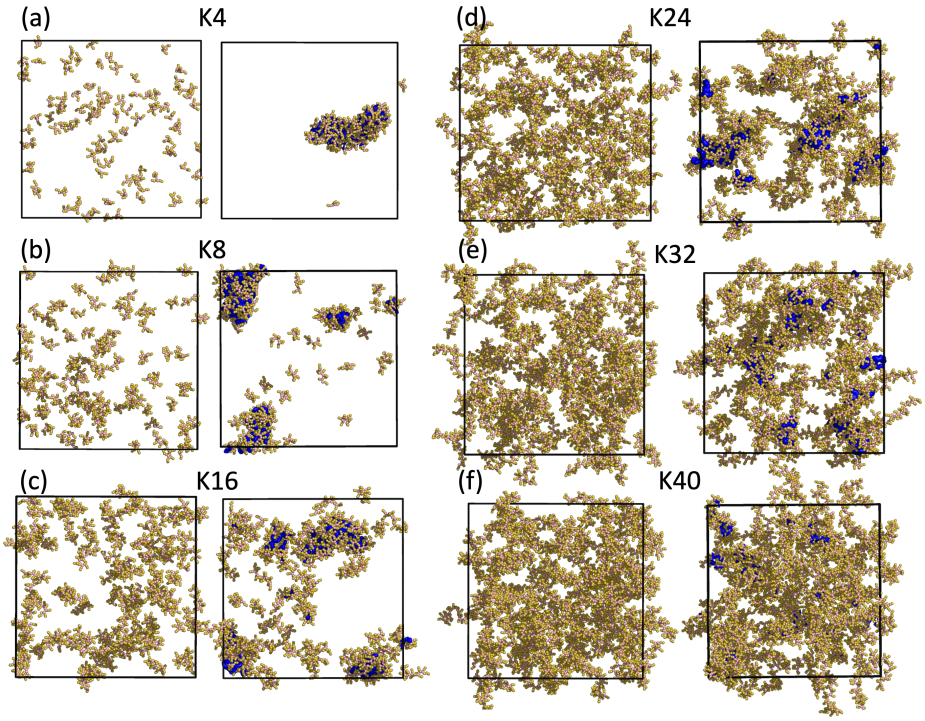

Figure S11: Final snapshots of the simulations containing 100 oligolysines of specific lengths, with maintained peptide concentration and ratio between oligolysine and ATPs. The left columns of (a-f) are representative snapshots without ATPs, while the right columns of (a-f) display representative snapshots with the addition of ATPs.

S13 Propensity of LLPS formation when restraining entropy

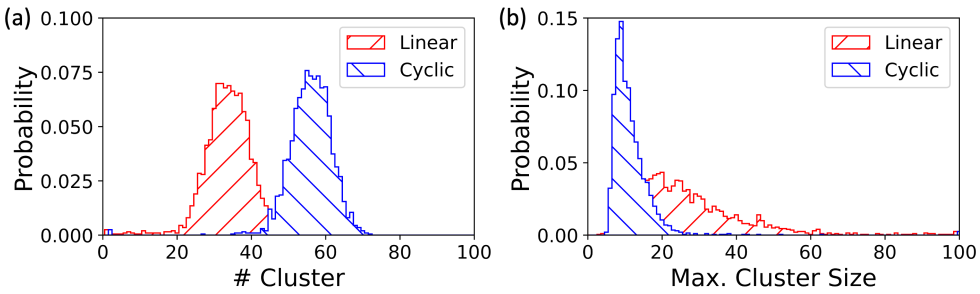

Figure S12: Propensity of forming LLPS in larger system of linear and cyclic oligolysines (the number was elevated up to 100 while maintaining similar peptide concentration) mixed with ATPs at the ionic concentration of 0.15 M: distribution of (a) the number of clusters and (b) the maximum cluster size.

S14 Propensity of LLPS formation when releasing entropy

S14.1 Results derived from systems of only 20 oligolysines

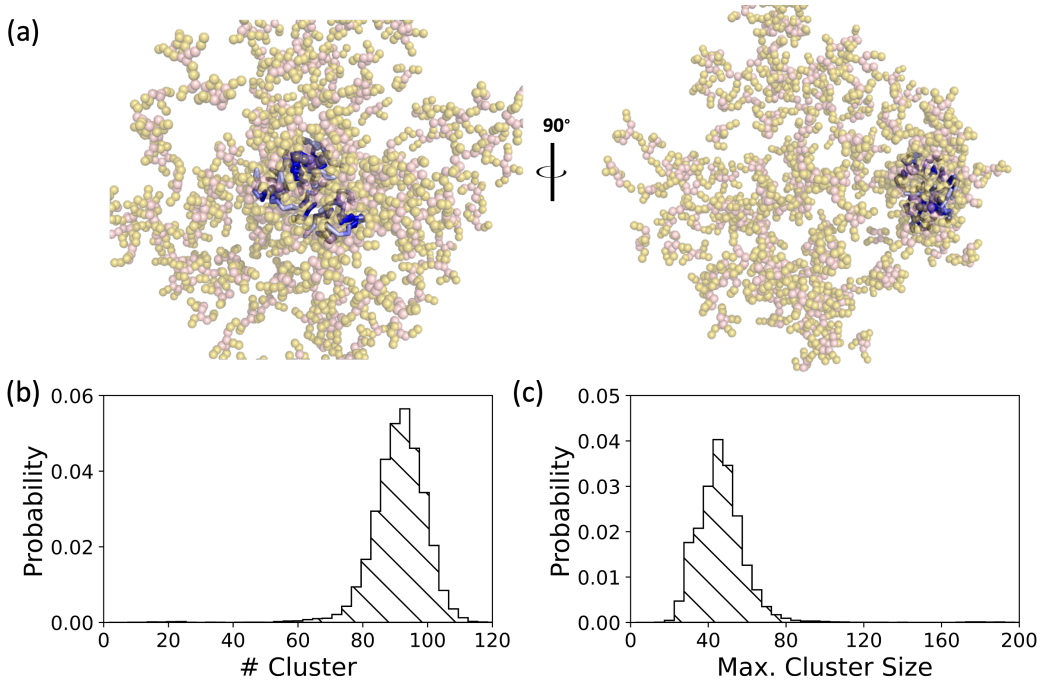

Figure S13: Propensity of forming LLPS when a linear peptide (K_{40}) was broken into 10 short oligolysine (K_4). (a) Representative snapshot; distribution of (b) the number of clusters and (c) the maximum cluster size.

S14.2 Results derived from large-size systems of 100 oligolysines and ATPs

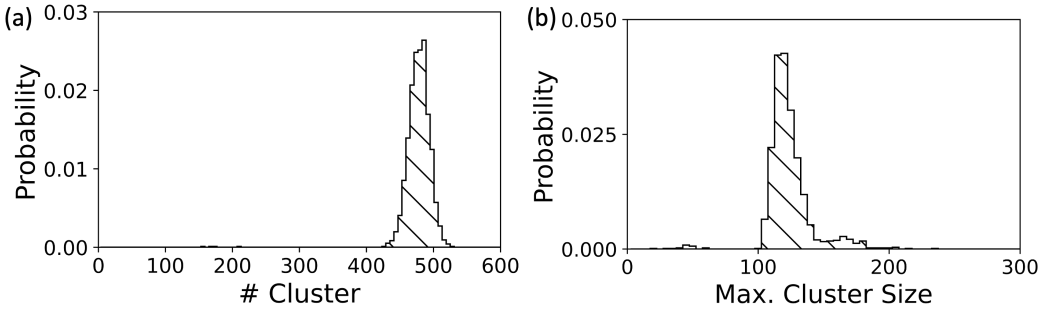

Figure S14: Propensity of forming LLPS when 100 linear peptide (K_{40}) was broken into 1000 short oligolysine (K_4). Distribution of (a) the number of clusters and (b) the maximum cluster size.

References

(1) Hanwell, M. D.; Curtis, D. E.; Lonie, D. C.; Vandermeersch, T.; Zurek, E.; Hutchison, G. R. Avogadro: an advanced semantic chemical editor, visualization, and analysis platform. *Journal of cheminformatics* **2012**, *4*, 1–17.

(2) de Jong, D. H.; Singh, G.; Bennett, W. D.; Arnarez, C.; Wassenaar, T. A.; Schafer, L. V.; Periole, X.; Tieleman, D. P.; Marrink, S. J. Improved parameters for the martini coarse-grained protein force field. *Journal of chemical theory and computation* **2013**, *9*, 687–697.

(3) Humphrey, W.; Dalke, A.; Schulten, K. VMD: visual molecular dynamics. *Journal of molecular graphics* **1996**, *14*, 33–38.